PHYSICAL REVIEW B **109**, 205132 (2024)

Collapse of quasiparticle multiplets and $5f$ itinerant-localized crossovers in cubic phase Pu_3Ga

Li Huang[*] and Haiyan Lu[†]

Science and Technology on Surface Physics and Chemistry Laboratory, P.O. Box 9-35, Jiangyou 621908, China

(Received 8 March 2021; revised 5 March 2024; accepted 25 April 2024; published 13 May 2024)

The high-temperature δ phase of plutonium can be stabilized at room temperature by doping it with a few-percent gallium, and the cubic phase Pu_3Ga plays a crucial role in understanding the mechanism of the stabilized δ phase of plutonium-gallium alloy. In this paper, we discovered that the spectral weights of $5f$ electrons in Pu_3Ga are reduced compared to δ-Pu, suggesting the increased localization of $5f$ electrons that promotes the stability of Pu_3Ga. Through a comprehensive investigation of the temperature-dependent correlated electronic states of Pu_3Ga using a combination of the density functional theory and the embedded dynamical mean-field theory, we found that the enhanced localization of $5f$ states at high temperatures is accompanied by depressing quasiparticle resonance peaks and weakened valence fluctuations. Moreover, the quasiparticle multiplets resulting from the many-body transitions among the $5f^4$, $5f^5$, and $5f^6$ electronic configurations collapse as temperature increases. The hybridizations between the $5f$ bands and conduction bands also decrease at high temperatures, causing changes in the Fermi surface geometry indicative of a temperature-driven electronic Lifshitz transition. Finally, the calculated linear specific heat coefficient γ is approximately 112 mJ / (mol K^2) at $T = 80$ K, suggesting that Pu_3Ga could be a promising candidate of plutonium-based heavy-fermion systems.

DOI: 10.1103/PhysRevB.109.205132

I. INTRODUCTION

In the partially filled $5f$ shell of actinides, the $5f$ electrons exhibit a fascinating and dualistic behavior, alternating between itinerant and localized states, thereby contributing to a wide array of intriguing lattice properties of the actinides [1]. For the early actinides (from Th to Np), the $5f$ electrons tend to be itinerant, actively participating in chemical bonding. This behavior typically results in the formation of very narrow and flat energy bands, leading to a notably high density of states near the Fermi level [2]. As these narrow $5f$ energy bands can be split by lattice distortions, effectively lowering the system's total energy, it is no wonder that the ground states of early actinides favor low-symmetry crystal structures. Conversely, the $5f$ electrons in the late actinides (from Am to No) have a propensity to become localized, rendering them chemically inert. This leads to the emergence of nontrivial local magnetic moments and nearly fixed atomic volumes [3]. Plutonium, as the sixth member of the actinide series (atomic No. 94, chemical symbol Pu), teeters on the brink between localized and itinerant $5f$ electronic states, displaying a rich array of exotic properties that warrant further exploration [4].

Plutonium is undoubtedly one of the most enigmatic and intricate elements in the periodic table [5]. Existing in six stable allotropes (α, β, γ, δ, δ', and ϵ phases) at ambient pressure [6], its crystal structures vary widely. The low-temperature α and β phases demonstrate monoclinic structures, while the high-temperature δ-Pu crystallizes in a face-centered cubic arrangement, boasting the largest atomic volume among the stable phases of Pu. Notably, from a lattice properties perspective, the δ phase stands out as particularly peculiar [5], wherein the volume contracts when heated, despite being a ductile phase. The magnetic behavior of plutonium has long confounded the condensed matter physics community. At low temperatures, its magnetic susceptibility is extraordinarily high and remains nearly constant, hinting at some form of magnetism. However, no long-range magnetic ordering has been observed in any phase of plutonium, even at extremely low temperatures [7,8]. Furthermore, the electrical resistivity of the δ phase surpasses that of other simple metals at room temperature by an order of magnitude, steadily increasing as the temperature drops to 100 K. The phonon dynamics and elastic properties of δ-Pu also exhibit remarkable characteristics [9,10]. The phonon dispersion curves of δ-Pu reveal pronounced softening along the transverse acoustic branch (i.e., the $T[111]$ mode), indicating lattice instability and suggesting the Bain path for the $\delta - \epsilon$ structural transition [11]. The nearly degenerate longitudinal and transverse acoustic phonon branches along the [001] direction result in approximately equal elastic constants C_{11} and C_{44}, yielding astonishing shear anisotropy (C'). In summary, the six stable allotropes of plutonium represent virtually distinct metals, each with entirely diverse $5f$ electronic structures [12–14].

The $5f$ electron wave functions, characterized by their extensive spatial reach and substantial overlap with *spd* conduction electron wave functions, enable active participation in chemical bonding [5]. Consequently, plutonium tends to form diverse intermetallic compounds [1]. One particularly scrutinized class of Pu-based materials is the Pu-Ga system, given its wide-ranging applications in military and energy industries [5]. While δ-Pu typically stabilizes at high temperatures, doping it with a few percent of trivalent metal impurities gallium

---

[*] lihuang.dmft@gmail.com

[†] hyluphys@163.com

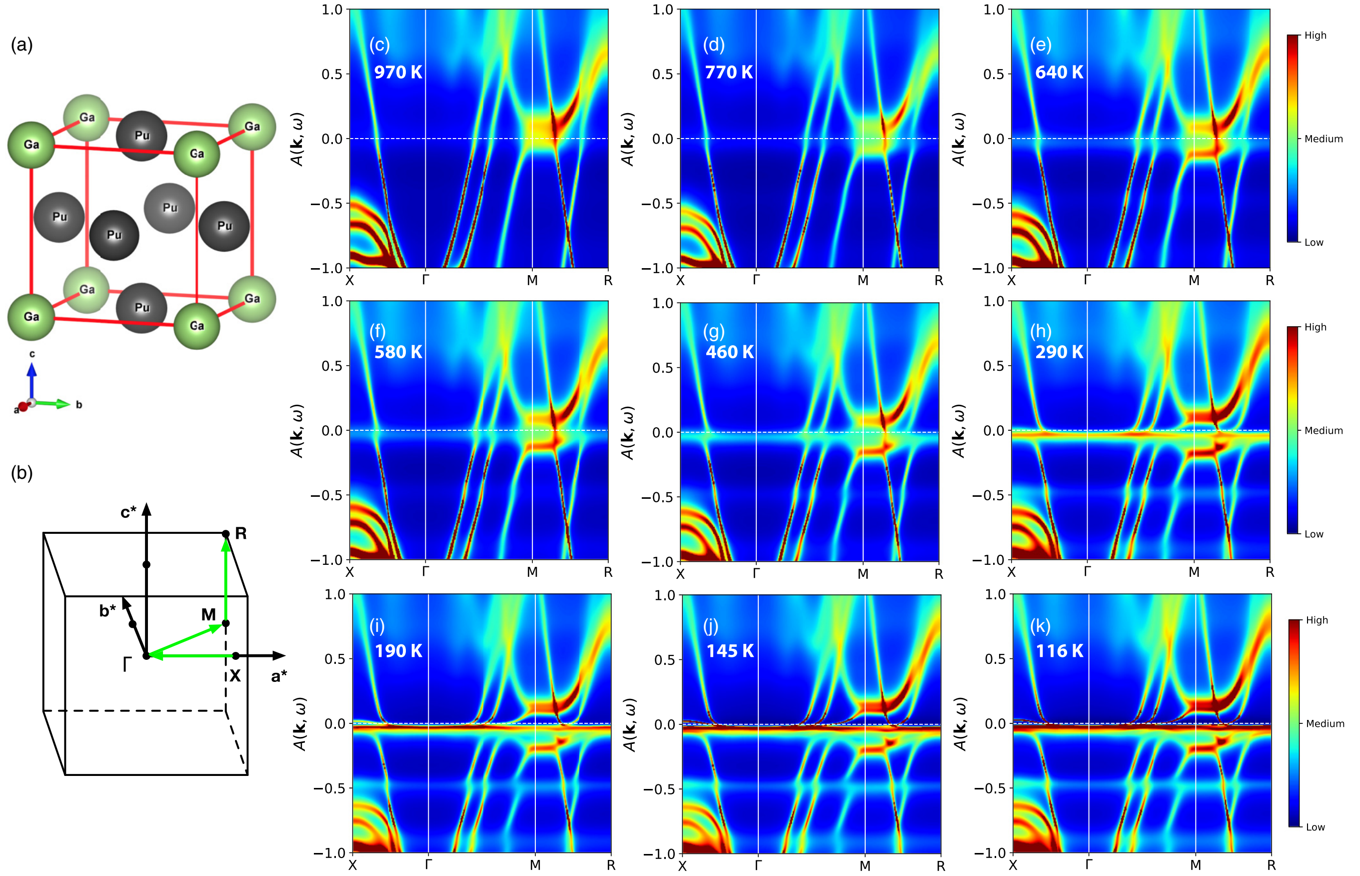

FIG. 1. Crystal structure and temperature-dependent quasiparticle band structures of cubic phase Pu_3Ga. (a) Schematic crystal structure of cubic phase Pu_3Ga. The Pu and Ga atoms are presented as grey and green balls, respectively. (b) The first Brillouin zone of cubic phase Pu_3Ga. The green arrows denote the high-symmetry directions ($X - \Gamma - M - R$) used in the following band structure calculations. (c)–(k) DFT + DMFT quasiparticle band structures of cubic phase Pu_3Ga calculated at various temperatures. In these panels, the horizontal dashed lines denote the Fermi level. When $T \leqslant 640$ K, distinct quasiparticle bands and hybridization gaps appear in the vicinity of the Fermi level.

(Ga) can extend its stability down to room temperature. The Pu-Ga phase diagram suggests that the δ phase Pu-Ga alloy may be metastable across a broad temperature range [6]. Despite the widespread use of the δ phase Pu-Ga alloy, the underlying mechanism behind the delay in the $\delta - \alpha$ phase transition and stabilization of the lattice by a few percent of Ga impurities remains a subject of intense and ongoing debate [15–21]. Beyond disorder in the Pu-Ga alloy, the Pu-Ga system comprises several intermetallic compounds, including PuGa (tetragonal), $PuGa_2$ (hexagonal), $PuGa_3$ (rhombohedral), $PuGa_3$ (hexagonal), $PuGa_4$ (orthorhombic), $PuGa_6$ (tetragonal), Pu_2Ga_3 (hexagonal), Pu_5Ga_3 (tetragonal), Pu_3Ga (tetragonal), and Pu_3Ga (cubic), among others [15].

Particularly, Pu_3Ga exists in two forms: an $AuCu_3$-type cubic phase [see Figs. 1(a) and 1(b)] at room temperature and a $SrSb_3$-type hexagonal phase at low temperatures, with the latter being a slight tetragonal deformation of the former along the c axis. When the atomic percentage of Ga in the δ phase Pu-Ga alloy is small ($<5\%$), the thermodynamically allowed decomposition into a mixture of α-Pu and the cubic phase Pu_3Ga at low temperatures occurs, although the equilibrium process can be very slow [6,15]. Recently, Li *et al.* used density functional theory plus U (static Coulomb interaction) to investigate the electronic and vibrational properties of the cubic phase Pu_3Ga [22]. Their findings highlighted strong hybridizations between Pu-$5f$, Pu-$6d$ states and the Ga-$3d$, Ga-$4p$ states. This suggests a significant influence of Ga impurities on the electronic structures of surrounding Pu atoms. Moreover, they observed conspicuous phonon softening in the transverse acoustic branch at the L point in the Brillouin zone. They attributed this phonon anomaly to the presence of Ga atoms, proposing that changes in electronic structures ultimately lead to alterations in lattice vibrations and phase stability of δ-Pu [22,23]. While this perspective appears reasonable, it faces challenges, as theoretical calculations predicted phonon softening in pure δ-Pu before any experimental observations [9–11]. Regardless, it is evident that understanding the $5f$ electronic structure is crucial for comprehending the structural, magnetic, transport, and lattice dynamics properties of plutonium and its intermetallic compounds. Therefore, to gain insights into the phase transitions and stability of the δ phase Pu-Ga alloy, a comprehensive understanding of the $5f$ electronic structure of the cubic phase Pu_3Ga is highly desired [6,15,24].

In the present paper, we have attempted to investigate the evolution of correlated electronic structures of cubic phase Pu_3Ga upon temperature by means of the density functional theory in combination with the embedded dynamical mean-field theory (DFT + DMFT) [25,26]. We found that at low temperature the 5f electrons in the cubic phase Pu$_3$Ga are itinerant, with remarkable quasiparticle multiplets near the Fermi level. As the temperature increases, 5f itinerant-localized crossover will occur, accompanied by a melting of the quasiparticle multiplets. During this electronic structure transition, the Fermi surface geometry, the 5f occupancy, and the hybridization gaps change accordingly.

II. METHODS

Since 5f electrons of Pu$_3$Ga are strongly correlated, a combination of DFT + DMFT is employed to treat the many-body interaction between 5f electrons. The DFT + DMFT method combines the DFT realistic band-structure calculation and a nonperturbative way to tackle the many-body local interaction effects in DMFT [25,26]. Then the DFT + DMFT approach is implemented into DFT and DMFT parts. In principle, the spin-orbit coupling and crystal field splitting should be treated on equal footing to accurately describe the 5f electronic states. Generally, the relativistic effect plays a crucial role in the electronic structure for the heavy elements with large spin-orbit coupling. Meanwhile, the crystal field splitting helps generate complicated magnetism [27]. For plutonium atom, the spin-orbit coupling is about 430 meV [28], which is larger than the crystal field splitting. So, to reduce the computing complexity and to improve the convergence efficiency, both strong electronic correlation and large spin-orbit coupling are considered in our calculations, but omitting the crystal field splitting.

A. DFT calculations

The DFT calculations were performed using the WIEN2K code, which implements a full-potential linearized augmented plane-wave formalism [29]. The experimental crystal structure of Pu$_3$Ga is adopted and the thermal expansion is ignored [22] within the temperature region considered. The radius of muffin-tin spheres for Pu and Ga atoms were chosen as 2.5 au and 2.1 au, respectively. In addition, $R_{\mathrm{MT}}K_{\mathrm{MAX}} = 8.0$. The 5$f$, 6$d$, and 7$s$ orbitals in Pu and 4f, 5d, and 6s orbitals in Ga were treated as valence states. The rest were treated as core states. The k mesh for Brillouin zone integration was $15 \times 15 \times 15$. The generalized gradient approximation, namely, the Perdew-Burke-Ernzerhof functional [30], was used to evaluate the exchange-correlation potential. The spin-orbit coupling effect was included in a variation manner. Since the calculation temperature is above the antiferromagnetic transition temperature of Pu$_3$Ga, the system was assumed to be nonmagnetic [22,23].

B. DFT + DMFT calculations

We utilized the eDMFT software package, developed by Haule *et al.*, to perform the DFT + DMFT calculations [31]. The many-body nature of the Pu-5f orbitals was captured by the DMFT formalism. The Coulomb interaction matrix for Pu-5f orbitals was constructed using the Slater integrals. The Coulomb repulsion interaction parameter U and Hund's exchange interaction parameter J_{H} are 5.0 eV and 0.6 eV, respectively, which were taken from Ref. [12]. We used the $|J, J_z\rangle$ basis to construct the local impurity Hamiltonian. A large energy window, from −10 eV to 10 eV with respect to the Fermi level, was used to build the DMFT projector, which was used to project the Kohn-Sham basis to local basis. The vertex-corrected one-crossing approximation (OCA) impurity solver [32] was employed to solve the resulting multiorbital Anderson impurity models. To reduce the computational consumption and accelerate the calculations, we have to truncate the Hilbert space of the local impurity problems. Only contributions from those atomic eigenstates with $N \in [3, 7]$ were retained during the calculations. The calculated results were also crosschecked by using the numerically exact and unbiased hybridization expansion version continuous-time quantum Monte Carlo impurity solver (dubbed CT-HYB) [33,34]. Then all the results concerning spectral functions and self-energies are obtained with OCA impurity solver. The double-counting term is used to cancel out the excess amount of electronic correlations that is already partly included in the DFT part. In the present paper, we just selected the fully localized limit scheme to describe the double-counting term [35]. It reads

$$\Sigma_{dc} = U\left(n_{5f} - \frac{1}{2}\right) - \frac{J_{\mathrm{H}}}{2}(n_{5f} - 1), \tag{1}$$

where n_{5f} is the nominal occupancy of Pu-5f orbitals. It was fixed to be 5.0 during the DFT + DMFT calculations. We conducted charge fully self-consistent DFT + DMFT calculations. About 60 ∼ 80 DFT + DMFT iterations were enough to obtain good convergence. The convergent criteria for charge density and total energy were 10^{-4} e and 10^{-5} Ry, respectively. It is worth noting that the direct output of the OCA impurity solver is real axis self-energy $\Sigma(\omega)$ which was used to calculate the momentum-resolved spectral functions $A(\mathbf{k}, \omega)$, density of states $A(\omega)$, renormalization factor Z, effective electron mass $m^\star$, Fermi surface, and other physical observables. For the three-dimensional Fermi surface, the energy bands that traverse the Fermi level are plotted as isoenergetic surface. Meanwhile, the two-dimensional Fermi surface is depicted only on the $k_x - k_y$ plane with $k_z = \pi/2$, which shall reveal the interior geometry of three-dimensional Fermi surface.

III. RESULTS

A. Quasiparticle band structures

The quasiparticle band structure (or, equivalently, momentum-resolved spectral function) $A(\mathbf{k}, \omega)$, which includes the one-particle vertex correction (i.e., the electron self-energy function), serves as a valuable theoretical tool for directly examining the status of the valence electrons of correlated electron materials. It can be validated by angle-resolved photoemission spectroscopy [36]. Here, the calculated $A(\mathbf{k}, \omega)$ along some selected high-symmetry directions in the irreducible Brillouin zone are illustrated in Figs. 1(c)–1(k). Clearly, the quasiparticle band structures of cubic phase Pu$_3$Ga are strongly temperature dependent. When the temperature is below 640 K, the 5f electrons become itinerant and form coherent hybridized bands. In the vicinity of the Fermi level (just 30 ∼ 40 meV below the Fermi energy), there are well-defined and nearly flat quasiparticle bands, which are likely connected with the itinerant 5f electrons [12]. These 5f quasiparticle

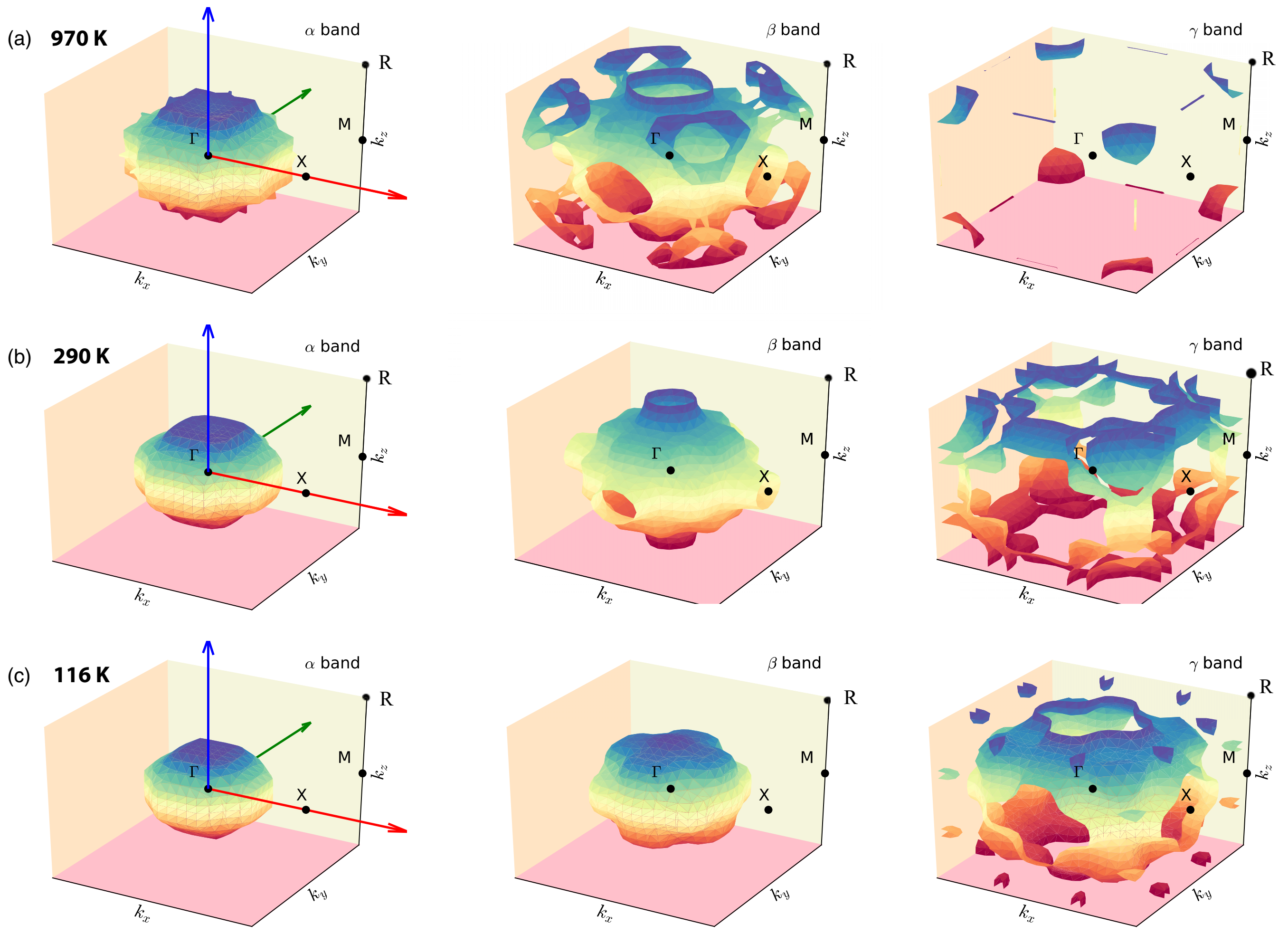

FIG. 2. 3D Fermi surfaces of cubic phase Pu_3Ga obtained by the DFT + DMFT method. (a) $T = 970$ K. (b) $T = 290$ K. (c) $T = 116$ K. There are three doubly degenerated bands (labeled α, β, and γ) crossing the Fermi level. They are plotted in the left, middle, and right columns, respectively.

bands strongly hybridize with the *spd* conduction bands, particularly along the $X - \Gamma$ and $\Gamma - M$ lines in the Brillouin zone. In addition, approximately 0.5 eV and 0.9 eV below the Fermi level, there are stripelike patterns in the spectra. It is speculated that these parallel features stem from the contributions of the spin-orbit splitting $5f_{5/2}$ and $5f_{7/2}$ states, respectively. When the temperature is higher than 640 K, the enhancing localization of $5f$ electrons leads to progressively incoherent spectra near the Fermi energy (see the band structures near the M point). The quasiparticle bands, the $c - f$ hybridizations, and the stripelike features diminish, indicating a temperature-driven itinerant-localized crossover for the $5f$ electrons. The coherent temperature T_{coh} marking the emergence of the quasiparticle bands and onset of the $c - f$ hybridizations is approximately 640 K. Finally, we note that the positions of the quasiparticle bands and stripelike features are hardly affected by the temperature in the low-temperature coherent states.

B. Fermi surface geometry

The evolution of $5f$ correlated electronic states will manifest itself in the Fermi surface geometry [37,38]. Figure 2 illustrates the three-dimensional Fermi surfaces of cubic phase Pu_3Ga at three representative temperatures. Three pairs of degenerate bands (number of bands: 26 and 27, 28 and 29, 30, and 31) are observed, labeled with the Greek letters α, β, and γ, respectively. The Fermi surfaces formed by the α bands exhibit an electronlike nature resembling distorted ellipsoids. With increasing temperature, their geometries remain unchanged, but their volumes increase. In contrast, the β and γ bands give rise to intricate Fermi surfaces with multiple sheets, and both their volumes and geometries are affected by temperature. To support this observation, two-dimensional Fermi surfaces are presented in Fig. 3 ($k_x - k_y$ planes intersecting $\Gamma - X - M$ cross section in Fig. 2). The crucial aspect is the behavior of the β bands. When $T \leqslant 190$ K, they intersect the $\Gamma - X$ line, forming ellipsoidlike Fermi surfaces [also seen in Fig. 2(c)], similar to the α bands. However, when $T \geqslant 290$ K, they intersect the $M - X$ line, resulting in a complete alteration of their Fermi surface geometries. In comparison with the evolution of the temperature-dependent electronic band structure in Fig. 1, it is evident that the number of bands crossing the Fermi level along the high-symmetry $\Gamma - X$ direction increases from one to two below 190 K. This implies an electronic Lifshitz transition for the $5f$ correlated

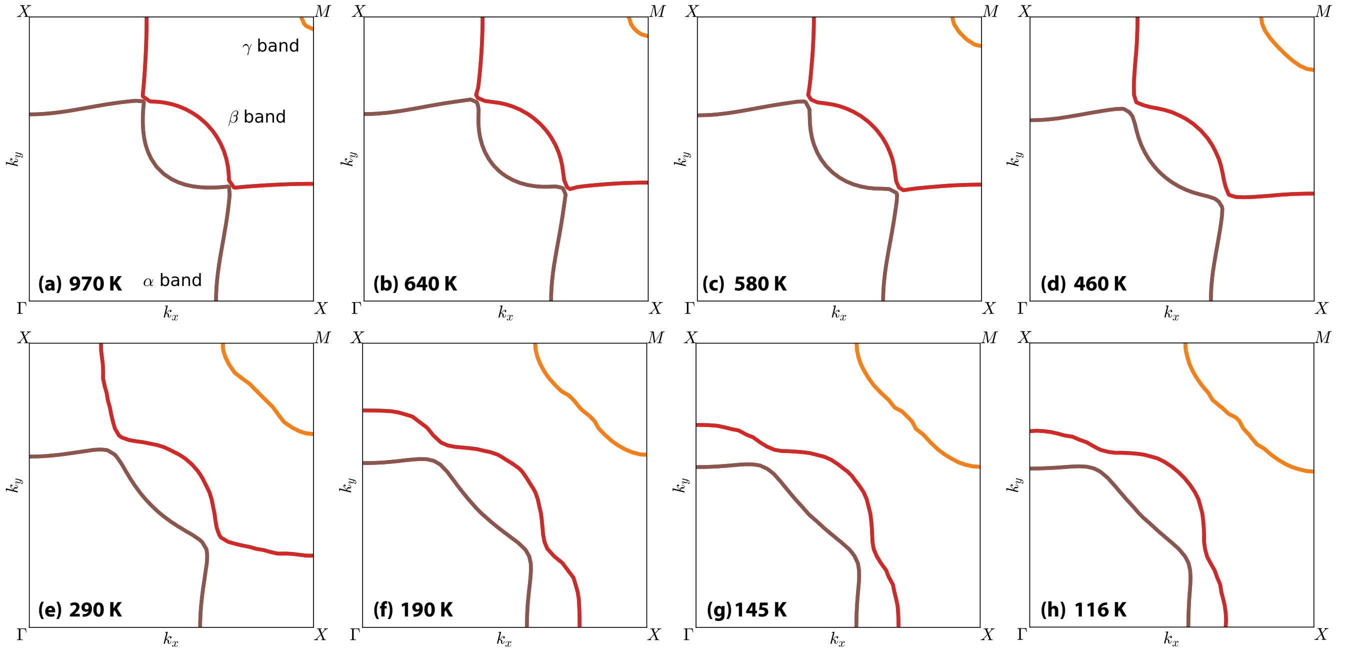

FIG. 3. 2D Fermi surfaces of cubic phase Pu$_3$Ga obtained by the DFT + DMFT method. In this figure, only the $k_x - k_y$ plane (with $k_z = \pi/2$) which intersects the Γ-X-M cross section in Fig. 2 is shown. There are three doubly degenerated bands (labeled α, β, and γ) traversing the Fermi level. They are visualized using different colors.

electronic states in the cubic phase Pu$_3$Ga between 190 K and 290 K, detectable through quantum oscillation experiments.

C. Density of states

Figures 4(a)–4(c) show the total density of states $A(\omega)$ and 5f partial density of states $A_{5f}(\omega)$ of cubic phase Pu$_3$Ga at three representative temperatures. Our calculations at 290 K reveal noticeable differences in the electronic density of Pu$_3$Ga compared to those calculated at zero temperature by using DFT+U method [22]. The main difference is that the Pu-5f electron density peak near the Fermi level is absent in Zhang *et al.*'swork, which is distinct from the representative peaks of 5f electronic states in δ-Pu. This discrepancy is likely related to the absence of temperature effects in DFT+U calculations and the underestimation of strong correlation properties among 5f electrons with the DFT+U method.

These spectra share some common characteristics. First, there are strong quasiparticle resonance peaks pinned at the Fermi level, which are associated with the nearly flat quasiparticle bands as already observed in the momentum-resolved spectral functions $A(\mathbf{k}, \omega)$ (see Fig. 1). Second, in Figs. 4(b) and 4(c), two discernible satellite peaks labeled P1 and P2 exist at −0.5 eV and −0.9 eV. These peaks are associated with the parallel stripelike features in $A(\mathbf{k}, \omega)$. Note that this three-peak structure (including P1, P2, and the central quasiparticle peak) that lies in the occupied states is quite common in Pu [12,28,39] and its intermetallic compounds, such as PuTe [40], PuCoIn$_5$ [41], and PuCoGa$_5$ [42,43]. In Ref. [40], Yee *et al.* named these peaks quasiparticle multiplets.

They proposed that the 5f valence fluctuations in conjunction with the atomic multiplet structures, which may be remarkable in some plutonium-based intermetallic compounds, could drive the demonstration of a multiplet of many-body quasiparticle peaks. On the other hand, Shick *et al.* proposed another analogous picture after they calculated the electronic structures of δ-Pu and PuB$_6$ with the DFT + DMFT method [43,44]. They found that the obtained spectral functions can be crudely split into two distinctive parts. Near the Fermi level, the well-pronounced atomic multiplet structures dominate. However, in the high-energy regime, the multiplets are merged into broad lower and upper Hubbard bands. Consequently, they called the materials that exhibit similar features the "Racah materials". In other words, δ-Pu belongs to the Racah metal, while PuB$_6$ is the Racah semiconductor or Racah insulator [43,44]. According to their definitions, we believe that the cubic phase Pu$_3$Ga belongs to the so-called Pu-based Racah metal. Third, there is a doublet of reflected peaks above the Fermi level. The positions of these peaks are approximately 0.4 eV and 0.8 eV. They are labeled as P3 and P4 in Figs. 4(b) and 4(c). Yee *et al.* predicted similar peaks in plutonium chalcogenides through a slave-boson analysis [40]. So, the fingerprint for the 5f photoemission spectra of cubic phase Pu$_3$Ga includes five peaks, i.e., a central quasiparticle peak and four satellites. The positions of these satellites are actually symmetric about the central quasiparticle peak.

Due to the spin-orbit coupling, the 5f orbitals are split into sixfold degenerated 5$f_{5/2}$ and eightfold degenerated 5$f_{7/2}$ states, respectively [1,12,13]. Then, to determine the orbital characters of the five characteristic peaks, we further calculated the j-resolved 5f partial density of states ($j = 5/2$ or 7/2). The results are depicted in Figs. 4(d)–4(f). Clearly, the central quasiparticle peak is mainly composed of the 5$f_{5/2}$ state. The 5$f_{7/2}$ state remains insulatinglike and manifests a gap in the Fermi level. The p1 peak is largely from the 5$f_{5/2}$

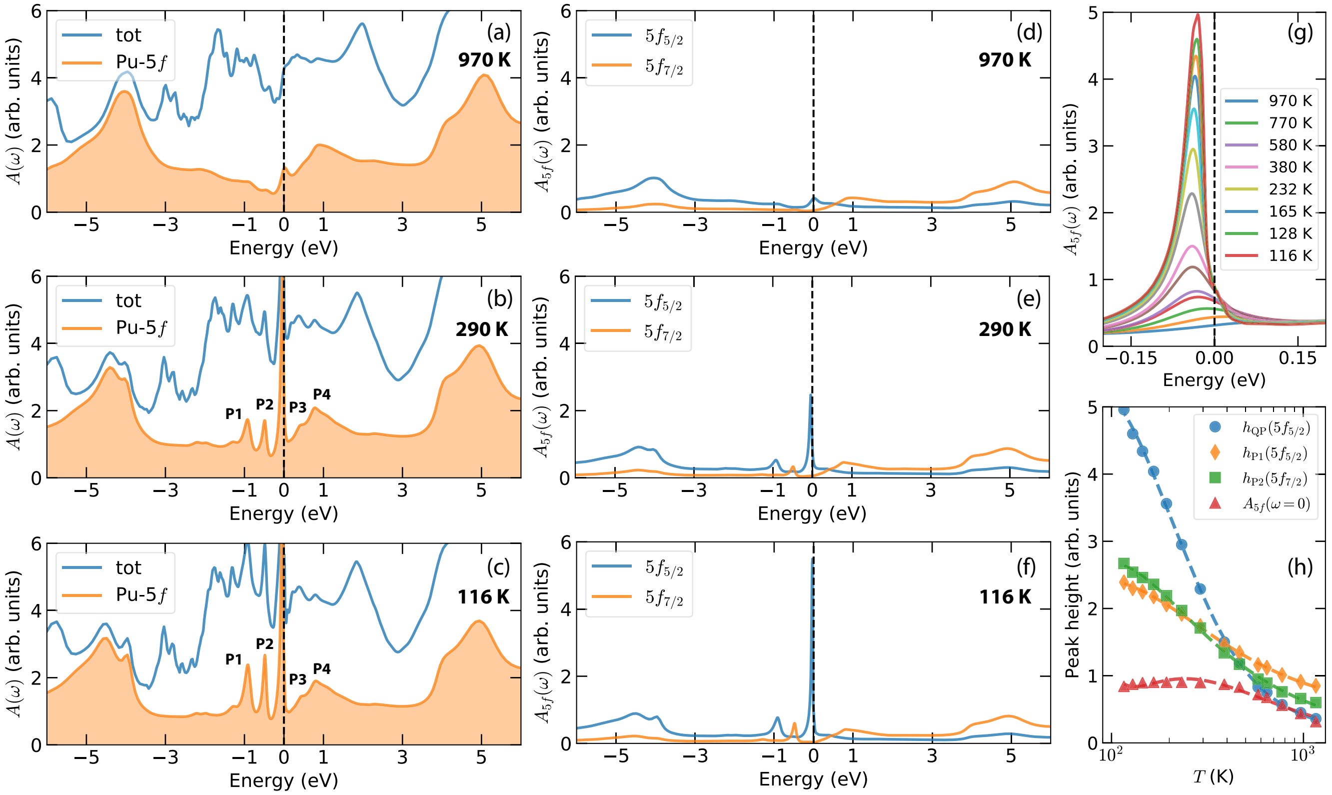

FIG. 4. Density of states of cubic phase Pu_3Ga obtained by the DFT + DMFT method. (a)–(c) Total density of states (solid lines) and $5f$ partial density of states (color-filled regions) of cubic phase Pu_3Ga at $T = 970$ K, 290 K, and 116 K. The peaks stemming from the quasiparticle multiplets are annotated with P1–P4. (d)–(f) The j-resolved $5f$ partial density of states [i.e., $A_{5f_{5/2}}(\omega)$ and $A_{5f_{7/2}}(\omega)$] of cubic phase Pu_3Ga at $T = 970$ K, 290 K, and 116 K. (g) Temperature-dependent central quasiparticle peaks (they are mainly comprised of the $5f_{5/2}$ states). From top to bottom, the system temperature T increases gradually (T is from 116 K to 970 K). (h) The height of the central quasiparticle peak $h_{\rm QP}(5f_{5/2})$, the height of the quasiparticle multiplet peak P1 $h_{\rm P1}(5f_{5/2})$, the height of the quasiparticle multiplet peak P2 $h_{\rm P2}(5f_{7/2})$, and the $5f$ spectral weight at the Fermi level $A_{5f}(\omega = 0)$ as a function of temperature T.

state, while for the other satellite peaks (P2–P4), they are built from $5f_{7/2}$ states.

Next, let us concentrate on the temperature dependence of these peaks. Figure 4(g) shows the temperature-dependent central quasiparticle peak. When the temperature is low, it should be a sharp and intense peak, indicating the itinerancy of the $5f$ electrons. On the contrary, this peak should be suppressed and finally disappear with increasing temperature, which signals localization of the $5f$ electrons and decay of the quasiparticles. Figure 4(h) shows spectral weights of the central quasiparticle peaks P1, and P2, and $A_{5f}(\omega)$ at $\omega = 0$ as a function of temperature. All of them decrease monotonically with respect to temperature. Notice that the spectral weights of P3 and P4 show the same trends (not shown in this figure). The strong temperature dependence of the five peaks implies that all of them originate from quasiparticle resonances [40,45]. In short, we find that with the increasing temperature, an orbital selective $5f$ itinerant-localized crossover would occur in the cubic phase Pu_3Ga.

D. Self-energy functions

It is generally believed that most of the electron correlation effects in correlated electron materials are encoded in their electron self-energy functions [25,26]. So, $\Sigma(\omega)$ were utilized to calculate quasiparticle weight Z and effective electron masses m^* for Pu-$5f$ electrons [26],

$$Z^{-1} = \frac{m^*}{m_e} = 1 - \frac{\partial \mathrm{Re}\Sigma(\omega)}{\partial \omega}\Big|_{\omega=0}, \tag{2}$$

where m_e denotes the mass of bare (noninteraction) electron. Figures 5(a) and 5(b) illustrate the renormalized imaginary parts of self-energy functions $Z|\mathrm{Im}\Sigma(\omega)|$ for the $5f_{5/2}$ and $5f_{7/2}$ states. Here, Z represents the quasiparticle weight or renormalization factor, indicating the strength of the electron correlation. Specifically, $Z|\mathrm{Im}\Sigma(0)|$ is considered a reflection of the low-energy electron scattering rate [39], which decreases rapidly as the temperature drops. Consequently, quasiparticles exhibit longer lifetimes and become coherent, often resulting in a reduction of electrical resistivity at low temperatures [46]. At low temperatures, both $Z|\mathrm{Im}\Sigma_{5f_{5/2}}(0)|$ and $Z|\mathrm{Im}\Sigma_{5f_{7/2}}(0)|$ approach zero. With an increase in temperature, they become finite values and increase quickly. Particularly, the quantitative coherent temperature can be derived from the self-energy functions. Figure 5(c) shows the imaginary parts of self-energy functions at the Fermi energy for the $5f_{5/2}$ states, i.e., $-\mathrm{Im}\Sigma_{5f_{5/2}}(\omega = 0)$ and the first derivative with respect to temperature, $-d\mathrm{Im}\Sigma_{5f_{5/2}}(\omega = 0)/d\ln T$, is also plotted. In comparison with Ce-based compounds [47] and UTe_2 [46], $-d\mathrm{Im}\Sigma_{5f_{5/2}}(\omega = 0)/d\ln T$ and its peak

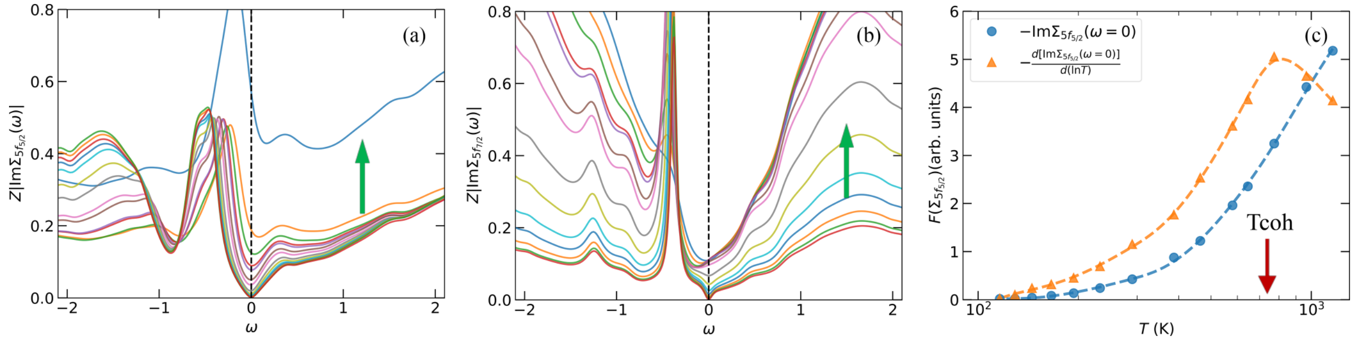

FIG. 5. Real-frequency self-energy functions of cubic phase $\mathrm{Pu_3Ga}$ obtained by the DFT + DMFT method. (a), (b) Temperature-dependent $Z|\mathrm{Im}\Sigma(\omega)|$ for the $5f_{5/2}$ and $5f_{7/2}$ states. Z means the renormalization factor. In these panels, the green arrows denote the increasing system temperature (T is from 116 K to 970 K). (c) $-d\mathrm{Im}\Sigma_{5f_{5/2}}(\omega=0)/d\ln T$ and $-\mathrm{Im}\Sigma_{5f_{5/2}}(\omega=0)$ as a function of temperature T, where the red arrows indicate the coherent temperatures [$T_{\mathrm{coh}}(5f_{5/2}) \approx 700$ K].

corresponds to the coherent temperature T_{coh}. When $T < T_{\mathrm{coh}}$, the electron coherence sets in and heavy electron states appear, leading to the rapid development of the quasiparticle peak near the Fermi level [36]. It is deduced that T_{coh} is about 700 K for the $5f_{5/2}$ state, which is roughly consistent with the value that is deduced from the spectral weights of the corresponding quasiparticle peaks [please refer to Figs. 4(g) and 4(h)]. Subsequently, it is proposed that the coherence temperature might guide the future electrical resistivity measurement.

E. Atomic eigenstate probabilities

δ-Pu exhibits characteristics of a mixed-valence metal, with its ground state representing a combination of different $5f$ electron configurations. This results in a significant deviation from the expected nominal value of 5.0 [7,12,28]. Interestingly, the cubic phase $\mathrm{Pu_3Ga}$ shares similarities with δ-Pu in terms of their spectral functions, including the notable three-peaks structure. This raises the question: Is the cubic phase $\mathrm{Pu_3Ga}$ also a mixed-valence metal? To address this inquiry, we aimed to quantify the probability (or time) that $5f$ electrons could reside in each atomic eigenstate. This computation involved projecting the DMFT ground state onto the $5f$ electron atomic eigenstates [40]. Suppose that p_Γ is the probability for the atomic eigenstate $|\Gamma\rangle$ and n_Γ is the number of electrons, then the $5f$ valence can be deduced by $\langle n_{5f}\rangle = \sum_\Gamma p_\Gamma n_\Gamma$ and the probability of $5f^n$ electronic configuration can be defined as $\langle w(5f^n)\rangle = \sum_\Gamma p_\Gamma \delta(n - n_\Gamma)$.

The resulting temperature-dependent $\langle n_{5f}\rangle$ and $\langle w(5f^n)\rangle$ with $5f^3 \sim 5f^7$ configurations are illustrated in Fig. 6. In the low-temperature regime, it is evident that the cubic phase $\mathrm{Pu_3Ga}$ behaves as a mixed-valence metal. Despite the dominance of the $5f^5$ configuration, significant contributions from the $5f^4$ and $5f^6$ configurations are observed. Valence fluctuations play a crucial role in generating the photoemission triplet below the Fermi level and influencing the effective $5f$ valence electrons. The obtained $\langle n_{5f}\rangle \approx 5.16$ is close to the values for δ-Pu [12,28] and PuTe [40]. However, this scenario changes in the high-temperature regime. At higher temperatures, there is a slight increase in the proportions of $5f^5$ and $5f^4$ configurations, while the $5f^6$ configuration decreases. This suggests restrained valence state fluctuation, with $5f$ valence electrons preferring the $5f^5$ and $5f^4$ con-

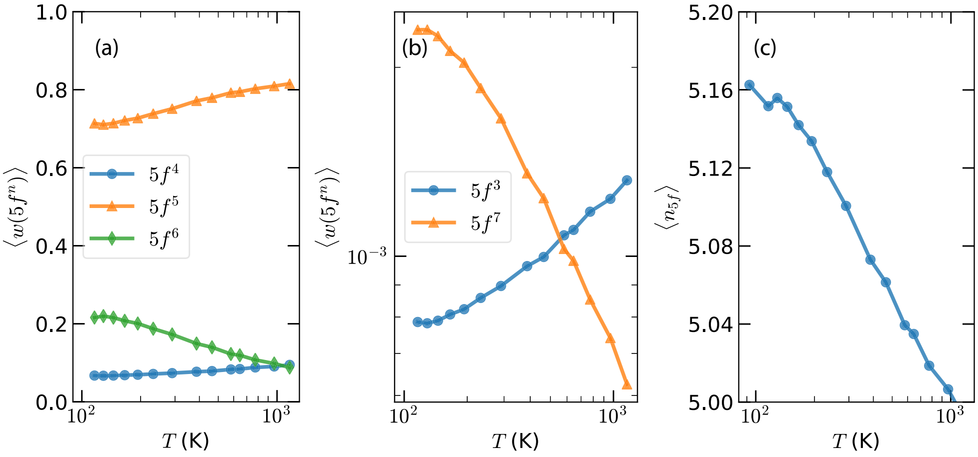

FIG. 6. Temperature-dependent valence state fluctuations and $5f$ occupancies of cubic phase $\mathrm{Pu_3Ga}$ obtained by the DFT + DMFT method. (a) Probabilities of $5f^4$, $5f^5$, and $5f^6$ electronic configurations as a function of temperature T. (b) Probabilities of $5f^3$ and $5f^7$ electronic configurations as a function of temperature T. (c) T-dependent $5f$ occupancies.

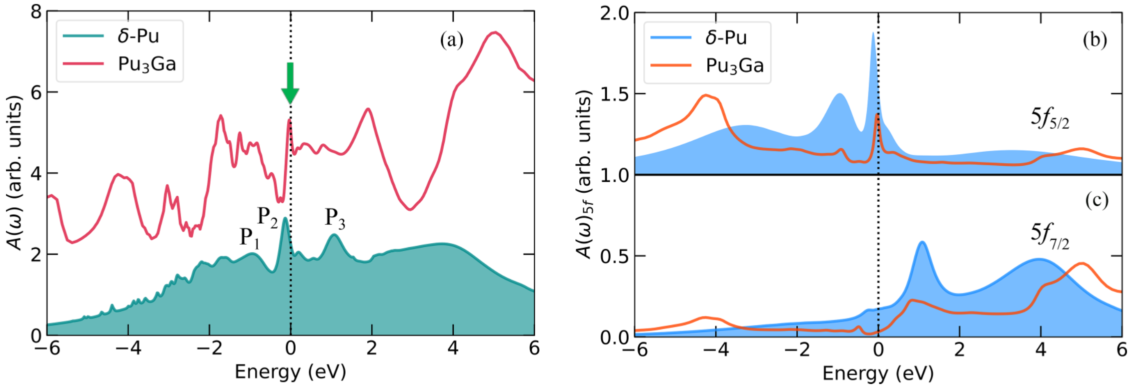

FIG. 7. Total density of states and $5f$ partial density of states of δ-Pu and Pu$_3$Ga obtained by DFT + DMFT method at 645 K. (a) Total density of states of δ-Pu (color-filled region) and Pu$_3$Ga (red solid line). The j-resolved $5f$ partial density of states $A_{5f_{5/2}}(\omega)$ (b) and $A_{5f_{7/2}}(\omega)$ (c) of δ-Pu (color-filled region) and Pu$_3$Ga (red solid line). The dotted line indicates the Fermi level and quasiparticle multiplet peaks of δ-Pu are marked P1–P3.

figurations. Additionally, the high-temperature effect shifts atomic multiplet energies, making valence fluctuation costly and suppressing quasiparticle multiplets. Consequently, the $5f$ electrons become more localized and the cubic phase Pu$_3$Ga transitions into an integral-valence metal ($\langle n_{5f}\rangle$ approaches its nominal value of 5.0).

IV. DISCUSSION

A. Comparison between Pu$_3$Ga and δ-Pu

To explore the underlying mechanism behind the Ga stabilized δ-Pu, it is insightful to compare the similarities and differences in the density of states. Given that δ-Pu stablizes at relatively high temperatures, we conducted density of states calculations at a typical temperature of 645 K using the OCA impurity solver. First, the main characteristics in the total density of states [see Fig. 7(a)] of Pu$_3$Ga are akin to those of δ-Pu. Notably, the total electronic density of δ-Pu exhibits a prominent Kondo resonance peak near the Fermi level, along with two "shoulder peaks" at approximately −1 eV and 1 eV relative to the Fermi level, primarily attributed to Pu-$5f$ electrons. This three-peak feature in the total density of states of δ-Pu has been verified by photoemission spectroscopy and previous theoretical calculations [28]. Upon comparison, the quasiparticle resonance peak of Pu$_3$Ga near the Fermi level is predominantly contributed by $5f$ electronic states of Pu. Moreover, the region below the Fermi level (approximately [−2 eV, −1 eV]) and above the Fermi level (approximately [1 eV, 2.5 eV]) embodies the hybridization between $5f$ states and conduction bands (Ga-$3d$ and Ga-$4p$ states).

Examining the $5f$ partial density of states [see Figs. 7(b) and 7(c)], both materials exhibit similar peak positions in the $5f$ density of states, albeit with different spectral weights. The main peak near the Fermi level and a shoulder peak at −1 eV are contributed by the $5f_{5/2}$ electronic state, while the $5f_{7/2}$ electronic state reveals a shoulder peak around 1 eV. Therefore, this typical three-peak structure related to the Pu-$5f$ electron atomic multiplets is classified as Racah material. The lower Hubbard band is identified in the broad peak around −5 eV to −3 eV, and the upper Hubbard band is recognized in the region approximately 4 eV to 6 eV. Importantly, the main distinction lies in the fact that the spectral weights of $5f_{5/2}$ and $5f_{7/2}$ electronic states in δ-Pu are higher than those in Pu$_3$Ga.

In summary, the hybridization of Pu-$5f$ electrons with Ga-$4p$ and Ga-$3d$ electrons in Pu$_3$Ga influences the density of states and hybridization functions. This is reflected in the reduction of spectral weights for $5f$ electrons of Pu$_3$Ga compared to δ-Pu, indicating the intensive localization of $5f$ states at high temperature 645 K. It should be pointed out that this picture aligns with the enhancement in the localized $5f$ states as temperature rises, which is depicted in Fig. 4. In addition, these results are consistent with previous studies on the charge transfer between Ga-$4p$ states and the corresponding Pu-$5f$ states [48] as well as the measured the Ga K-edge extended x-ray absorption fine structure in a Pu-Ga alloy [49]. In comparison with the high-temperature stable δ-Pu, whose $5f$ states are localized than the room-temperature stable α phase [12], the localized $5f$ states might contribute to stabilizing the crystal structure of Pu$_3$Ga.

B. Evolution of hybridization gap

As already illustrated in Figs. 1(c)–1(k), there exists strong hybridization between the $5f$ bands and the conduction bands as temperature is below the coherent temperature $T < T_{\text{coh}}$. The $c-f$ hybridization induces a hybridization gap which is close to the Fermi level, so as to affect the physical properties of Pu$_3$Ga. Thus, it is constructive to elaborate ob the temperature dependence of hybridization gap. Phenomenologically, the low-energy hybridized bands can be well described by a simple mean-field hybridization band picture (i.e., the periodical Anderson model) [36]. Within this picture, the energy dispersions read

$$E_{\pm}(k) = \frac{[\epsilon_0 + \epsilon(k)] \pm \sqrt{[\epsilon_0 - \epsilon(k)]^2 + 4|V_k|^2}}{2}, \quad (3)$$

where ϵ_0 means the renormalized $5f$ energy level, $\epsilon(k)$ is the unrenormalized band dispersion for conduction electrons, and V_k is the hybridization strength. On the left side of this equation, the "+" and "–" symbols denote the upper and lower branches of hybridized bands, respectively. Figure 8(a)

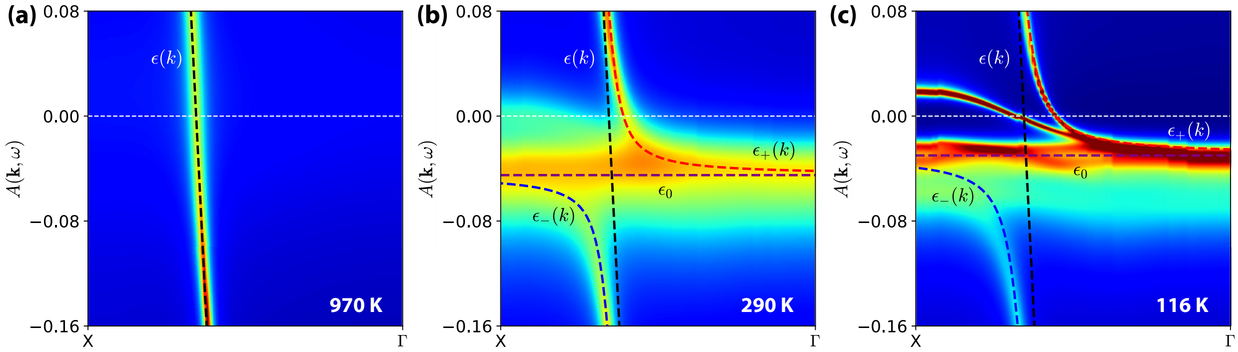

FIG. 8. Temperature-dependent quasiparticle band structures (along the $X-\Gamma$ direction) of cubic phase Pu_3Ga obtained by the DFT + DMFT method. (a) $T = 970$ K. (b) $T = 290$ K. (c) $T = 116$ K. The white horizontal dashed lines denote the Fermi level. Here, we utilized a periodical Anderson model [see Eq. (3)] to fit the low-energy band structures. The colorful dashed lines are the fitting results.

represents the band dispersion at $T = 970$ K. At high temperature, the 5f partial electronic state density of Pu shows that the 5f electrons near the Fermi energy develop a very small spectral weight, indicating strong localization of 5f electrons. Therefore, it is believed that the 5f electrons are unlikely to participate in chemical bonding, so the hybridization is usually negligible (i.e., $|V_k| = 0$ and $\epsilon_0 = 0$), then Eq. (3) is simplified to $E_\pm(k) = \epsilon(k)$. Therefore, we employed the data at $T = 970$ K to calibrate $\epsilon(k)$ (see the black dashed lines in Fig. 8). Figures 8(b) and 8(c) show the band structures at $T = 290$ K and 116 K, respectively. Fitting Eq. (3) gives $\epsilon_0 = -45$ meV and $|V_k| = 100$ meV for $T = 290$ K, and $\epsilon_0 = -30$ meV and $|V_k| = 120$ meV for $T = 116$ K. Consequently, the direct hybridization gaps ($\Delta \approx 2|V_k|$) are 200 meV at 290 K, and 240 meV at 116 K, respectively. The hybridization gaps suggest that the high-temperature effect will push the 5f energy level away from the Fermi level, so as to restrain the $c-f$ hybridization and subsequently reduce the hybridization gap. Besides the hybridized bands considered here, there also exist hybridizations between the quasiparticle multiplets and conduction bands. At this point, the mechanism behind the multiband hybridization phenomenon and anisotropy in f-electron systems remains under investigation and lacks complete clarification [50]. Therefore, the general physical depiction in our paper suggests that the hybridization gap qualitatively enlarges with decreasing temperature, but it does not offer a quantitative description of the formation of hybridization gaps. It is expected that the intricate temperature-driven hybridization dynamics of Pu-based compounds shall be conducted in the future.

C. Electronic heat capacity

The heat capacity of materials can be expressed as $C_v(T) = \gamma T + \beta T^3$, where the linear term γT comes from the contribution of electronic part and γ is called the linear specific heat coefficient. Within the Fermi-liquid theory, γ is given by the following equation:

$$\gamma = \pi k_B^2 \sum_\alpha \frac{A_\alpha(0)}{Z_\alpha}, \tag{4}$$

where α is the orbital index, $A_\alpha(0)$ is the spectral weight at the Fermi level, and Z_α is the orbital-resolved renormalization factor [26,45]. Usually, large γ [$\gamma > 100$ mJ / (mol K^2)] is regarded as a useful indicator to distinguish the heavy-fermion metals from normal metals. We ignored the contributions from conduction bands and assumed that the system is in the Fermi-liquid state when $T < T_{\rm coh}$. The calculated γ is about 112 mJ / (mol K^2) at $T = 80$ K, which is almost double the value of δ-Pu [$\gamma = 64 \pm 3$ mJ / (mol K^2) as $T \to 0$ K] [51]. Therefore, it is supposed that the cubic phase Pu_3Ga may be a promising candidate of Pu-based heavy-fermion system [52].

To summarize, we employed an advanced first-principles many-body approach to investigate the electronic structures of cubic phase Pu_3Ga. We focused on the temperature dependence of the correlated electronic states. When the temperature rises, the itinerant-localized crossover for Pu-5f electrons occur successively, giving rise to the collapse of the quasiparticle multiplets, closure of the hybridization gaps, and alterations in the Fermi surface geometry. The calculated linear specific heat coefficient γ was found to be remarkable [$\gamma > 100$ mJ / (mol K^2)], suggesting Pu_3Ga as a potential candidate for Pu-based heavy-fermion materials. Our results provide a comprehensive view of how the 5f correlated electronic states evolve concerning temperature in Pu-based materials. Additionally, these findings shed light on the intricate electronic structures of the Pu-Ga system. Further studies about the other Pu-Ga intermetallic compounds will be undertaken.

ACKNOWLEDGMENTS

This work is supported by the National Natural Science Foundation of China under Grants No. 12274380, No. 11934020, and No. 2022YFA1402201), CAEP Project No. TCGH0710, and Innovation Foundation of CAEP (No. CX20210033).

APPENDIX

Band structure calculated with CT-HYB and OCA impurity solver

To verify the accuracy of our calculations using the OCA impurity solver, it is essential to conduct a detailed comparison of the electronic band structure of Pu_3Ga obtained from both the CT-HYB and OCA impurity solvers. Figure 9(a) depicts the electronic band structure of Pu_3Ga at 116 K calculated with CT-HYB impurity solver, while Fig. 9(b) represents

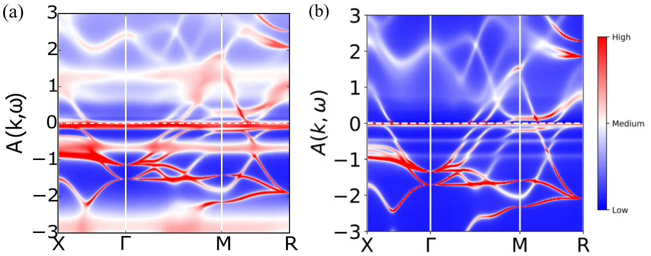

FIG. 9. Electronic band structure of Pu_3Ga at 116 K obtained by CT-HYB impurity solver (a) and OCA impurity solver (b).

the results obtained with OCA impurity solver. The band structure is plotted along the high-symmetry k-points X-Γ-M-R. Generally, the main characteristics of the electronic band structure are consistent between the two methods. Apparently, the Pu-$5f$ electronic bands exhibit higher spectral weights near the Fermi level, leading to hybridization with the conduction electrons and the opening of a band gap. Particularly, within an energy range of approximately (−2 eV, −1 eV) below the Fermi level, the flat Pu-$5f$ electronic bands become evident. Especially at the Γ point, there exists an electron-type band below the Fermi level. Furthermore, the conduction bands are almost identical both above and below the Fermi level, although a slight difference is noticeable in energy range from −3 eV to 1 eV, attributed to some incoherent energy bands formed by the conduction states. Overall, the electronic band structure computed using the OCA impurity solver is comparable to that from the CT-HYB impurity solver.

The OCA impurity solver incorporates a specific type of vertex correction, excluding diagrams containing a line with more than one crossing, and the third order shows nearly quantitative consistency with CT-HYB results for localized correlated $5f$ electrons [53]. In this context, the OCA impurity solver is highly accurate in many correlated systems with narrow bands. For instance, it provides the exact critical U in the Hubbard model and an accurate Kondo scale in the Kondo lattice model [31]. Therefore, we consider the results obtained using the OCA impurity solver in our study to be reliable, and we utilized these results to reduce the computational workload.

[1] K. T. Moore and G. van der Laan, Nature of the $5f$ states in actinide metals, Rev. Mod. Phys. **81**, 235 (2009).

[2] P. Söderlind, O. Eriksson, B. Johansson, J. M. Wills, and A. M. Boring, A unified picture of the crystal structures of metals, Nature (London) **374**, 524 (1995).

[3] S. Heathman, R. G. Haire, T. Le Bihan, A. Lindbaum, K. Litfin, Y. Méresse, and H. Libotte, Pressure induces major changes in the nature of americium's $5f$ electrons, Phys. Rev. Lett. **85**, 2961 (2000).

[4] R. C. Albers, Condensed-matter physics: An expanding view of plutonium, Nature (London) **410**, 759 (2001).

[5] *Challenges in Plutonium Science*, Los Alamos Science, Number 26, edited by N. G. Cooper (Los Alamos National Laboratory, 2000).

[6] S. S. Hecker, The magic of plutonium: $5f$ electrons and phase instability, Metall. Mater. Trans. A **35**, 2207 (2004).

[7] M. Janoschek, P. Das, B. Chakrabarti, D. L. Abernathy, M. D. Lumsden, J. M. Lawrence, J. D. Thompson, G. H. Lander, J. N. Mitchell, S. Richmond, M. Ramos, F. Trouw, J.-X. Zhu, K. Haule, G. Kotliar, and E. D. Bauer, The valence-fluctuating ground state of plutonium, Sci. Adv. **1**, e1500188 (2015).

[8] J. C. Lashley, A. Lawson, R. J. McQueeney, and G. H. Lander, Absence of magnetic moments in plutonium, Phys. Rev. B **72**, 054416 (2005).

[9] X. Dai, S. Y. Savrasov, G. Kotliar, A. Migliori, H. Ledbetter, and E. Abrahams, Calculated phonon spectra of plutonium at high temperatures, Science **300**, 953 (2003).

[10] J. Wong, M. Krisch, D. L. Farber, F. Occelli, A. J. Schwartz, T.-C. Chiang, M. Wall, C. Boro, and R.-Q. Xu, Phonon dispersions of fcc δ-Plutonium-Gallium by inelastic x-ray scattering, Science **301**, 1078 (2003).

[11] R. J. McQueeney, A. C. Lawson, A. Migliori, T. M. Kelley, B. Fultz, M. Ramos, B. Martinez, J. C. Lashley, and S. C. Vogel, Unusual phonon softening in δ-phase plutonium, Phys. Rev. Lett. **92**, 146401 (2004).

[12] L. Huang and H.-Y. Lu, Nature of the $5f$ electronic structure of plutonium, Phys. Rev. B **101**, 125123 (2020).

[13] W. H. Brito and G. Kotliar, Correlation strength and orbital differentiation across the phase diagram of plutonium metal, Phys. Rev. B **102**, 245111 (2020).

[14] N. Lanatà, Y.-X. Yao, C.-Z. Wang, K.-M. Ho, and G. Kotliar, Phase diagram and electronic structure of praseodymium and plutonium, Phys. Rev. X **5**, 011008 (2015).

[15] S. S. Hecker, D. R. Harbur, and T. G. Zocco, Phase stability and phase transformations in Pu–Ga alloys, Prog. Mater. Sci. **49**, 429 (2004).

[16] B. Sadigh and W. G. Wolfer, Gallium stabilization of δ-Pu: Density-functional calculations, Phys. Rev. B **72**, 205122 (2005).

[17] P. Söderlind, A. Landa, J. E. Klepeis, Y. Suzuki, and A. Migliori, Elastic properties of Pu metal and Pu-Ga alloys, Phys. Rev. B **81**, 224110 (2010).

[18] G. Robert, A. Pasturel, and B. Siberchicot, Thermodynamic, alloying and defect properties of plutonium: Density-functional calculations, J. Alloys Compd. **444-445**, 191 (2007).

[19] C.-M. Li, R. Yang, B. Johansson, and L. Vitos, Anomalous thermodynamic properties and phase stability of δ-$Pu_{1-x}M_x$ (M=Ga and Al) alloys from first-principles calculations, Phys. Rev. B **94**, 214108 (2016).

[20] K. T. Moore, P. Söderlind, A. J. Schwartz, and D. E. Laughlin, Symmetry and stability of δ plutonium: The influence of electronic structure, Phys. Rev. Lett. **96**, 206402 (2006).

[21] P. Söderlind and B. Sadigh, Density-functional calculations of α, β, γ, δ, δ', and ϵ plutonium, Phys. Rev. Lett. **92**, 185702 (2004).

[22] M.-L. Li, Y. Yang, F. Zheng, and P. Zhang, Electronic and vibrational properties of Pu_3Ga: A theoretical explanation for the phonon softening observed in Pu-Ga alloys, Phys. Rev. B **96**, 134102 (2017).

[23] M.-L. Li, Y. Yang, F.-W. Zheng, C. Wang, and P. Zhang, Electronic and vibrational properties of Pu_3M (M=Al, Ga, In, and Tl): A first-principles study, Phys. Rev. B **100**, 184101 (2019).

[24] R.-S. Li, X. Lu, D.-Q. Xin, J.-T. Wang, and B.-Y. Ao, Magnetic order and valence fluctuation in a Pu-Ga intermetallic compound studied via a first principles calculation, Int. J. Quantum Chem. **120**, e26105 (2020).

[25] G. Kotliar, S. Y. Savrasov, K. Haule, V. S. Oudovenko, O. Parcollet, and C. A. Marianetti, Electronic structure calculations with dynamical mean-field theory, Rev. Mod. Phys. **78**, 865 (2006).

[26] A. Georges, G. Kotliar, W. Krauth, and M. J. Rozenberg, Dynamical mean-field theory of strongly correlated fermion systems and the limit of infinite dimensions, Rev. Mod. Phys. **68**, 13 (1996).

[27] N. Lanatà, Y.-X. Yao, X.-Y. Deng, V. Dobrosavljević, and G. Kotliar, Slave boson theory of orbital differentiation with crystal field effects: Application to UO_2, Phys. Rev. Lett. **118**, 126401 (2017).

[28] J. H. Shim, K. Haule, and G. Kotliar, Fluctuating valence in a correlated solid and the anomalous properties of δ-plutonium, Nature (London) **446**, 513 (2007).

[29] P. Blaha, K. Schwarz, G. Madsen, D. Kvasnicka, and J. Luitz, WIEN2k, An augmented plane wave + local orbitals program for calculating crystal properties (Karlheinz Schwarz, Techn. Universität Wien, Austria, 2001).

[30] J. P. Perdew, K. Burke, and M. Ernzerhof, Generalized gradient approximation made simple, Phys. Rev. Lett. **77**, 3865 (1996).

[31] K. Haule, C.-H. Yee, and K. Kim, Dynamical mean-field theory within the full-potential methods: Electronic structure of $CeIrIn_5$, $CeCoIn_5$, and $CeRhIn_5$, Phys. Rev. B **81**, 195107 (2010).

[32] K. Haule, S. Kirchner, J. Kroha, and P. Wölfle, Anderson impurity model at finite Coulomb interaction U: Generalized noncrossing approximation, Phys. Rev. B **64**, 155111 (2001).

[33] K. Haule, Quantum Monte Carlo impurity solver for cluster dynamical mean-field theory and electronic structure calculations with adjustable cluster base, Phys. Rev. B **75**, 155113 (2007).

[34] E. Gull, A. J. Millis, A. I. Lichtenstein, A. N. Rubtsov, M. Troyer, and P. Werner, Continuous-time Monte Carlo methods for quantum impurity models, Rev. Mod. Phys. **83**, 349 (2011).

[35] V. I. Anisimov, F. Aryasetiawan, and A. I. Lichtenstein, First-principles calculations of the electronic structure and spectra of strongly correlated systems: the LDA + U method, J. Phys.: Condens. Matter **9**, 767 (1997).

[36] S. Kirchner, S. Paschen, Q.-Y. Chen, S. Wirth, D.-L. Feng, J. D. Thompson, and Q.-M. Si, Colloquium: Heavy-electron quantum criticality and single-particle spectroscopy, Rev. Mod. Phys. **92**, 011002 (2020).

[37] R. M. Tutchton, W.-T. Chiu, R. C. Albers, G. Kotliar, and J.-X. Zhu, Electronic correlation induced expansion of Fermi pockets in δ-plutonium, Phys. Rev. B **101**, 245156 (2020).

[38] C.-C. Joseph Wang, M. D. Jones, and J.-X. Zhu, Fermi surface topology and de Haas–van Alphen orbits in $PuIn_3$ and $PuSn_3$ compounds, Phys. Rev. B **88**, 125106 (2013).

[39] W. H. Brito and G. Kotliar, Site and orbital selective correlations in β-Pu, Phys. Rev. B **99**, 125113 (2019).

[40] C.-H. Yee, G. Kotliar, and K. Haule, Valence fluctuations and quasiparticle multiplets in plutonium chalcogenides and pnictides, Phys. Rev. B **81**, 035105 (2010).

[41] J.-X. Zhu, P. H. Tobash, E. D. Bauer, F. Ronning, B. L. Scott, K. Haule, G. Kotliar, R. C. Albers, and J. M. Wills, Electronic structure and correlation effects in $PuCoIn_5$ as compared to $PuCoGa_5$, Europhys. Lett. **97**, 57001 (2012).

[42] W. H. Brito, S. Choi, Y. X. Yao, and G. Kotliar, Orbital-dependent correlations in $PuCoGa_5$, Phys. Rev. B **98**, 035143 (2018).

[43] A. B. Shick, J. Kolorenc, J. Rusz, P. M. Oppeneer, A. I. Lichtenstein, M. I. Katsnelson, and R. Caciuffo, Unified character of correlation effects in unconventional Pu-based superconductors and δ-Pu, Phys. Rev. B **87**, 020505(R) (2013).

[44] A. B. Shick, L. Havela, A. I. Lichtenstein, and M. I. Katsnelson, Racah materials: Role of atomic multiplets in intermediate valence systems, Sci. Rep. **5**, 15429 (2015).

[45] C. A. Marianetti, K. Haule, G. Kotliar, and M. J. Fluss, Electronic coherence in δ-Pu: A dynamical mean-field theory study, Phys. Rev. Lett. **101**, 056403 (2008).

[46] Y.-J. Xu, Y.-T. Sheng, and Y.-F. Yang, Quasi-two-dimensional Fermi surfaces and unitary spin-triplet pairing in the heavy fermion superconductor UTe_2, Phys. Rev. Lett. **123**, 217002 (2019).

[47] J. H. Shim, K. Haule, and G. Kotliar, Modeling the localized-to-itinerant electronic transition in the heavy fermion system $CeIrIn_5$, Science **318**, 1615 (2007).

[48] S. C. Hernandez, D. S. Schwartz, C. D. Taylor, and A. K. Ray, Ab initio study of gallium stabilized δ-plutonium alloys and hydrogen-vacancy complexes, J. Phys.: Condens. Matter **26**, 235502 (2014).

[49] P. G. Allen, A. L. Henderson, E. R. Sylwester, P. E. A. Turchi, T. H. Shen, G. F. Gallegos, and C. H. Booth, Vibrational properties of ga-stabilized δ-Pu by extended x-ray absorption fine structure, Phys. Rev. B **65**, 214107 (2002).

[50] Z.-Z. Wu, Y. Fang, H. Su, W. Xie, P. Li, Y. Wu, Y.-B. Huang, D.-W. Shen, B. Thiagarajan, J. Adell, C. Cao, H.-Q. Yuan, F. Steglich, and Y. Liu, Revealing the heavy quasiparticles in the heavy-fermion superconductor $CeCu_2$ Si_2, Phys. Rev. Lett. **127**, 067002 (2021).

[51] J. C. Lashley, J. Singleton, A. Migliori, J. B. Betts, R. A. Fisher, J. L. Smith, and R. J. McQueeney, Experimental electronic heat capacities of α- and δ-plutonium: Heavy-fermion physics in an element, Phys. Rev. Lett. **91**, 205901 (2003).

[52] E. D. Bauer and J. D. Thompson, Plutonium-based heavy-fermion systems, Annu. Rev. Condens. Matter Phys. **6**, 137 (2015).

[53] Q. Yin, A. Kutepov, K. Haule, G. Kotliar, S. Y. Savrasov, and W. E. Pickett, Electronic correlation and transport properties of nuclear fuel materials, Phys. Rev. B **84**, 195111 (2011).